bioRxiv preprint doi: https://doi.org/10.1101/2020.02.28.969139; this version posted March 25, 2020. The copyright holder for this preprint (which was not certified by peer review) is the author/funder, who has granted bioRxiv a license to display the preprint in perpetuity. It is made available under aCC-BY 4.0 International license.

Multithreaded two-pass connected components labelling and particle analysis in ImageJ

Michael Doube[1]

1. Department of Infectious Diseases and Public Health, City University of Hong Kong, Tat Chee Avenue, Kowloon, Hong Kong SAR

Abstract

Sequential region labelling, also known as connected components labelling, is a standard image segmentation problem that joins contiguous foreground pixels into blobs. Despite its long development history and widespread use across diverse domains such as bone biology, materials science, and geology, connected components labelling can still form a bottleneck in image processing pipelines. Here, I describe a multithreaded implementation of classical two-pass sequential region labelling and introduce an efficient collision resolution step, '*bucket fountain*'. Code was validated on test images and against commercial software (Avizo). It was performance tested on images from 2 MB (161 particles) to 6.5 GB (437,508 particles) to determine whether theoretical linear scaling (O(n)) had been achieved, and on 1 – 40 CPU threads to measure speed improvements due to multithreading. The new implementation achieves linear scaling (b = 0.918 – 1.068, $time \propto pixels^b$; R^2 = 0.985 – 0.998), which improves with increasing thread number up to 8-10 threads, suggesting that it is memory bandwidth limited. This new implementation of sequential region labelling reduces the time required from hours to a few tens of seconds for images of several GB, and is limited only by hardware scale. It is available open source and free of charge in BoneJ.

Introduction

Region labelling is a standard segmentation problem in 2D and 3D image processing, in which groups of pixels that form contiguous domains are identified and each discrete domain is given a unique label [1]. Region labelling is needed across disciplines, for example to identify pores in sintered polymers [2], soil [3], rock [4,5], cement [6], noodle dough [7], teeth [8] or bone [9], from images obtained by modalities such as X-ray microtomography (XMT), confocal microscopy, or serial sectioning microscopy. It is also useful to perform region labelling to remove small particles from images prior to calculating the Euler characteristic of a connected structure, for example to calculate trabecular bone's connectivity density (Conn.D), a measure of the number of trabecular struts [10]. XMT images on contemporary instruments are often circa 2048^3 pixels, or larger after stitching of projections or image stacks. Parallelised connected components labelling algorithms have existed for at least the last 30 years [11], yet slow region labelling can still be an obstruction to measuring features of interest in a timely manner, especially on large 3D image data.

Various multithreaded, chunked, single-threaded and mapped region labelling algorithms were included in BoneJ [12] from its earliest releases and improvements made in subsequent years. The starting point for these algorithms was the 3D Object Counter ImageJ plugin [13] published open source by Cordelières and Jackson (reported in [14]). The 3D Object Counter was a naïve and recursive implementation that scaled as ~$O(n^2)$ because every time a label change occurred, all the image pixels were iterated to update matching labels. For small images of the order a few tens of MB, processing times were tolerable, but for larger images of hundreds of MB and above, processing times became prohibitive.

Alternative approaches that avoid recursion such as *breadth-first* and *depth-first* flood fill algorithms [1] record the coordinates of foreground pixels and may function adequately for small images, but used on large images can consume a prohibitive amount of memory. In these algorithms, every 1-byte foreground pixel is represented by 12 bytes of coordinate data (3 dimensions × 4-byte integers), which can easily exceed available system memory for larger images. More complex two-pass approaches record collisions between neighbouring pixel subregions during

bioRxiv preprint doi: https://doi.org/10.1101/2020.02.28.969139; this version posted March 25, 2020. The copyright holder for this preprint (which was not certified by peer review) is the author/funder, who has granted bioRxiv a license to display the preprint in perpetuity. It is made available under aCC-BY 4.0 International license.

the first pass, resolve the collisions in an intermediate step, and merge connected subregions in the second pass. The network of collisions may be visualised as a graph, with subregion labels as nodes and the collision as an edge connecting two adjacent subregion labels [1]. Because each pixel is accessed a fixed number of times, two-pass approaches have the potential to scale linearly (as $O(n)$) and thus perform well on large data, provided that label collision resolution is efficient. Improvements to linear speed should also be possible by multithreading the two pass algorithm, however, collisions between threads during label collision recording and resolution require either synchronisation of data access or careful design to ensure threads never read and write the same data at the same time.

This report proposes a multithreaded implementation of two-pass sequential region labelling with efficient collision resolution and tests the hypotheses 1) that linear scaling ($O(n)$) is achieved and 2) that further linear speed improvements may be achieved as number of processor threads increases.

Installation and code availability

The current implementation has been developed in the Java programming language for the popular scientific image processing platform ImageJ [15]. The simplest and recommended way to install the software is by installing the Fiji Is Just ImageJ (Fiji) [16] bundle from https://fiji.sc/, and adding the BoneJ update site to Fiji according to the instructions at https://imagej.net/BoneJ2. This installs the command *Particle Analyser* in the user menus, which can be found using the keyboard shortcut [L] or using the search bar in the ImageJ GUI.

Code changes are tracked using Git [17], and published at GitHub (https://github.com/bonej-org/BoneJ2), while release version code is archived at Zenodo under a BSD 2-clause licence (see Data Availability). In BoneJ1, all methods were contained in a single class, `ParticleCounter`. The current release achieves separation of concerns by creating three new classes: `ConnectedComponents` (labels regions); `ParticleAnalysis` (measures region features); `ParticleDisplay` (handles graphical output); leaving `ParticleCounter` as a 'master' plugin that coordinates user input and output with ImageJ's API and the 3 new classes. `ConnectedComponents` is intended to be reused by other ImageJ plugins via its public `run()` method.

Description of the algorithm

Input data

The algorithm expects a 2D or 3D image that has been segmented into foreground and background. In ImageJ this is a 8-bit binary image that contains only 0 and 255. Other numbers of dimensions could conceivably work with the current approach, provided that suitable neighbourhoods and multithreading chunking strategies are devised.

First pass

The first pass proceeds as described in the classical algorithm [1] with some important variations. An ID value is initialised with a value of 1 to increment region labels. Label 0 is reserved for background. A neighbourhood that checks only previously-visited pixels iterates through all the pixels in a raster pattern, labelling the current pixel with the smallest label value found among the neighbouring pixels. If no smaller label than ID is found, the current pixel is set to ID and ID incremented by 1. Label pixels are stored in a primitive integer array that has the same dimensions as the input image (Fig 1a).

In preparation for later collision resolution, the neighbourhood pixel values are added to an `ArrayList` of `HashSets`, which can be visualised as a column of numbered buckets (Fig. 1b). The position (index) of a bucket (`HashSet`) in the column (`ArrayList`) relates to a region label. The contents of each bucket are neighbouring labels. Each bucket is initialised containing one label matching the bucket's position in the column. During the first pass, the bucket with its position

bioRxiv preprint doi: https://doi.org/10.1101/2020.02.28.969139; this version posted March 25, 2020. The copyright holder for this preprint (which was not certified by peer review) is the author/funder, who has granted bioRxiv a license to display the preprint in perpetuity. It is made available under aCC-BY 4.0 International license.

matching each neighbour pixel is looked up and the current pixel's label added to it. An efficiency is gained by skipping background neighbours, neighbours matching the current pixel, and neighbours that are the same as the last neighbour to be added. Because the current pixel's label is always less than or equal to the neighbours' labels, buckets receive only labels that have lower values than the buckets' positions. Use of `HashSets` prevents the same label from being added to a bucket more than once. It is not necessary to store pairs of labels as nodes and edges, as described in the classical algorithm.

Collision resolution

The presence of labels within a bucket means that all the labels belong to the same region. Although it helps to consider the underlying graph structure of the labels in a region, there is no need to reconstruct the specific connections among labels and these individual relations are ignored. If a label is found in more than one bucket, then the contents of all buckets containing that label can be aggregated into a single bucket. The first step in this algorithm's collision resolution allows labels to flow downwards into lower buckets, merging buckets' contents on the way, which is somewhat like the flow of water in the kinetic sculpture *Bucket Fountain* by Burren & Keen (1969) installed in Cuba Mall, Wellington, New Zealand. Starting from the highest bucket and proceeding to the lowest bucket, all the labels in each bucket are checked (Fig 1c-f). If labels are found that are lower than the bucket's position, the bucket is emptied into the lower bucket whose position equals the lowest label in the upper bucket. Later in the iteration the lower bucket will have all its labels checked, and all of the labels that have accumulated in it from higher buckets may be emptied into another, lower, bucket. Implementing buckets as `HashSets` means that each time a bucket pours its labels into another bucket, redundant labels are eliminated. In the final state, all the buckets have been checked and the labels in a bucket are all greater than or equal to the bucket position, which is the opposite to the starting state.

The *bucket fountain* does not always merge labels that are transitively connected (Fig 1f). A second step checks consistency by iterating back up through the buckets ensuring that labels are always bigger than the bucket number, and that each label appears exactly once within the whole set of buckets. If either condition is not satisfied, the offending bucket is emptied as before, into the bucket matching the lowest label. Consistency is checked in this manner in a `while()` loop, until no inconsistencies are found, typically with two and sometimes three iterations. During this process, labels are paired with the lowest label in their bucket, and a look-up table (LUT) is constructed that translates the first-pass label to a final label. Each bucket (`HashSet`) is paired with its minimum label in a `HashMap`. A second `HashMap` associates first pass labels and the minimum replacement label. The `hashMap`'s set of first pass labels is checked against the replacement label stored in the `lutMap` to ensure that the first pass label is being minimised. Once the labels are minimised within buckets, the content of each bucket represents the complete set of first pass labels that represent each region. Gaps between buckets are removed by assigning consecutive labels to a new `HashMap` `lutLut`, which is then copied to the final LUT, which is implemented as a primitive integer array for efficient storage and addressing. Making a LUT from the collision resolution diverges from the Burger & Burge pseudocode, which looks up replacement labels from the HashSet during pixel iteration.

Second pass

In the second pass, each first pass label is read from the label array and replaced by the value held at the label's position in the LUT.

Multithreading

Because this algorithm contains minimal recursion through pixels there is little need for synchronisation, leading to the ability to implement a multithreading strategy exploiting the implementation of *xy* image slices as independent arrays within the 2D image stack array (Fig 1a,b).

bioRxiv preprint doi: https://doi.org/10.1101/2020.02.28.969139; this version posted March 25, 2020. The copyright holder for this preprint (which was not certified by peer review) is the author/funder, who has granted bioRxiv a license to display the preprint in perpetuity. It is made available under aCC-BY 4.0 International license.

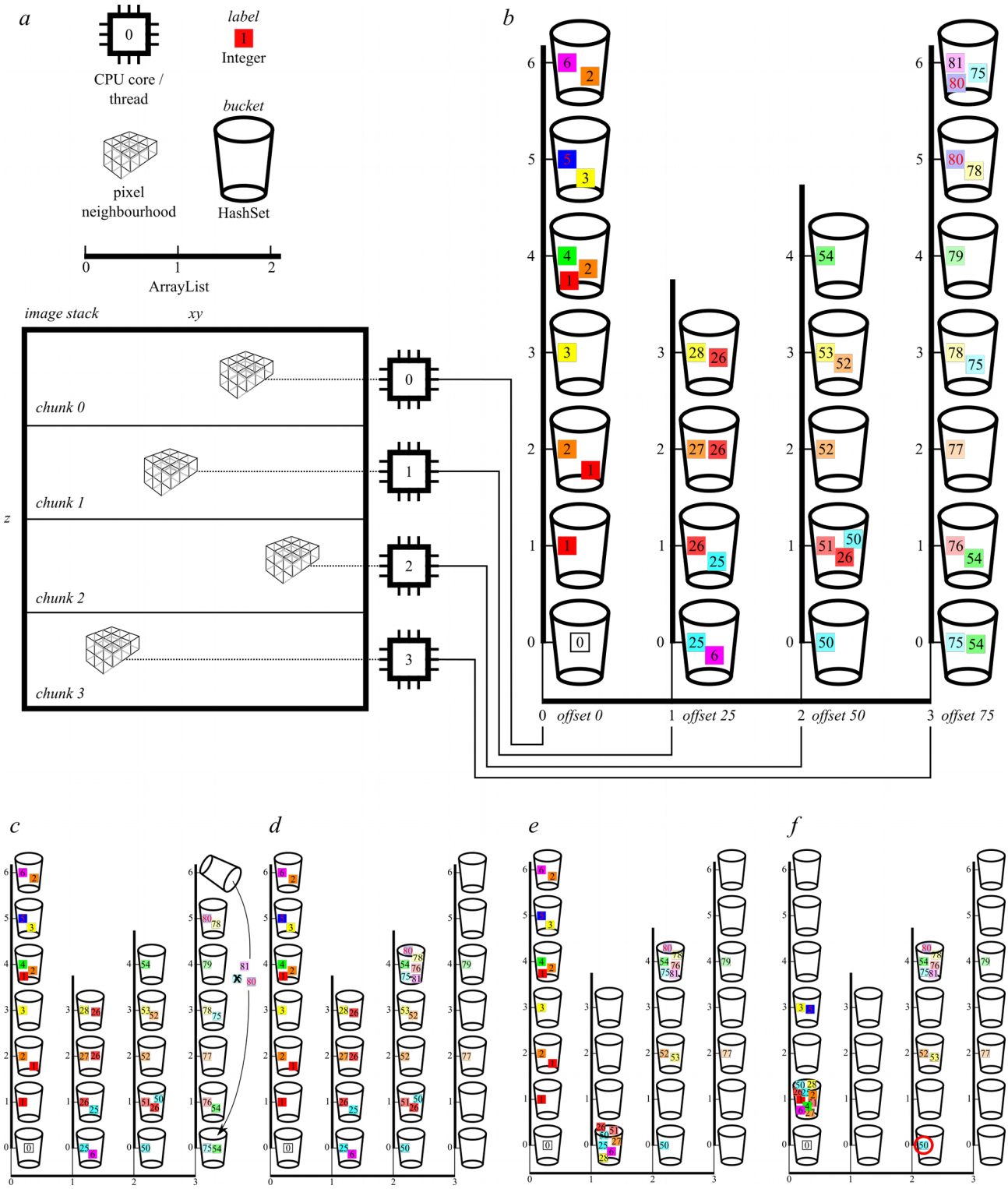

Figure 1: Visual summary of the first pass and of bucket fountain collision resolution. a) half-neighbourhoods, one per thread and one thread per image chunk, raster over the image pixels b) each thread addresses its own column of buckets, adding to the bucket that matches the neighbourhood centre pixel the labels of the other neighbours, which always have lower values than the centre pixel. Each bucket always contains its own label, and is created only once needed. In this example a total label range of 100 is split over 4 chunks giving each chunk a label range of 25, and offsets of 0, 25, 50 and 75, which keep each chunk's label range separate from the others' ranges. c) the bucket fountain starts on the highest valued bucket and descends towards 0, pouring labels into the bucket matching the lowest label contained in the bucket. Redundant labels [here, 75] are eliminated. Intermediate steps (d, e) demonstrate the state after emptying all buckets from the 3rd column and down to the first bucket of the first column. f) the state after completion of bucket fountain. Note the orphaned label 50 with red outline in column 2, which is picked up by the subsequent consistency and LUT-creation step. In this toy example, bucket fountain results in simplification of 40 labels spread over 19 buckets into 23 labels in 7 buckets, with one orphan.

bioRxiv preprint doi: https://doi.org/10.1101/2020.02.28.969139; this version posted March 25, 2020. The copyright holder for this preprint (which was not certified by peer review) is the author/funder, who has granted bioRxiv a license to display the preprint in perpetuity. It is made available under aCC-BY 4.0 International license.

In the first pass the label image is considered as a series of chunks, each chunk relating to a discrete range in *z*. Each chunk or *z*-range is processed in a separate thread. To ensure that the label space of each chunk does not interfere with the label space of the other chunks, each chunk is assigned a range of labels, calculated as the maximum label divided by the number of chunks. A special neighbourhood that does not check the previous chunk's last slice is used on the zeroth slice of each chunk, then the usual half-neighbourhood is used for the rest of the chunk. After the whole chunk is processed, the zeroth slice is processed again using the half-neighbourhood, which detects collisions between particle labels in the last slice of the previous chunk and particle labels in the zeroth slice of the current chunk.

Each chunk's collisions are stored in an independent list (`ArrayList<ArrayList<HashSet<Integer>>>`) to avoid synchronisation overhead and concurrent modification of elements (Fig 1b). A label offset equal to the minimum of the chunk's label space is used to relate bucket positions, which have zero-based numbering, to labels, which are label offset indexed. This allows the full range of labels to be used without creating unneeded `HashSets`. During collision resolution, labels belonging to the prior chunk are readily recognised because they are less than the chunk's label offset. Collision resolution is performed in a single thread, and the second pass is performed in multiple threads using the same chunked *z*-range strategy as in the first pass. The final LUT is a 2D `int` array, with each chunk having its own 1D LUT, and the index for the look-up value being calculated by subtracting the chunk label offset from the label being replaced.

Foreground versus background

This algorithm can work with any neighbourhood configuration. The current implementation assumes a 26-connected foreground. Its complementary 6-connected background is used during a particle filtering step prior to calculating connectivity, implemented as Purify in BoneJ [12,18].

Analysis and Display

Analysis and Display options are selected by the user in a single step via a GUI dialog, called on an open image by a single menu command. All user options are displayed in one setup dialog and no further user interaction required to generate output images and data. The intention is to minimise menu clicking and GUI interaction, which can represent a substantial time cost to users. Reproducibility and efficiency may be enhanced by recording and running a macro script, which avoids repeated GUI clicking and can be run as a batch over many input images or incorporated into a larger workflow.

Individual particles are identified by their unique label in the label array and a binary copy, limited to the particle's extent in *x*, *y*, and *z*, is used for input to BoneJ's other analysis methods. These include connectivity [18], local thickness [19], volume, surface area, moments of inertia, skeleton branch count and total length [20], and best fit ellipsoids, as described and validated elsewhere for single structures [12]. Any 3D binary operation available in the ImageJ plugin ecosystem could readily be applied to each particle. Particles may be displayed in stacks by their label, size, thickness, or in 3D as voxel volumes or surface meshes. Analysis results, such as best fit ellipsoids, may also be displayed as stacks or in the 3D Viewer [21].

Validation and Performance Testing

Simple validation was performed with a test script that generated a stack containing cubes, some with voids. An image of a single spiral in *xz* passing through multiple image chunks several times (Fig. 2a) was used to ensure that merging discrete particle subregions across image chunks completed successfully. A 7×10^9-pixel XMT image of particles (*s10up*) was obtained from the BoneJ user community and cropped into four smaller volumes, of 2, 16, 128 and 1024 MB (Fig 2b),

bioRxiv preprint doi: https://doi.org/10.1101/2020.02.28.969139; this version posted March 25, 2020. The copyright holder for this preprint (which was not certified by peer review) is the author/funder, who has granted bioRxiv a license to display the preprint in perpetuity. It is made available under aCC-BY 4.0 International license.

to cover 4-5 orders of magnitude of pixel number, with which the scaling characteristics of the algorithm were measured. All test images and scripts are available online (see Data Availability).

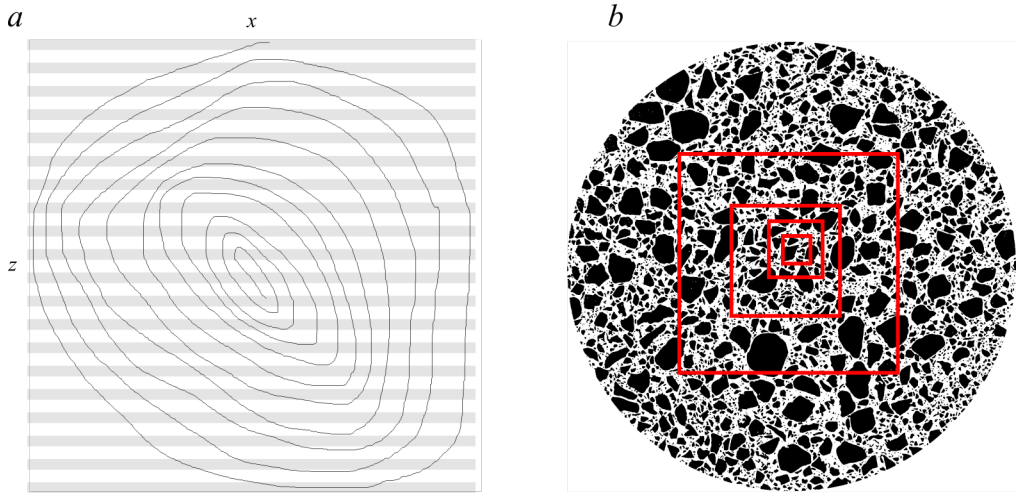

Figure 2: Test images. a) a spiral in *xz* (image dimensions 1024 × 3 × 1024 pixels) passing through multiple chunks tests the ability of the algorithm to connect subregions that are connected through multiple transitive steps via multiple chunks. Chunks are indicated by pale grey and white horizontal stripes. b) *s10up*, a binarised XMT scan of a particulate material (2103 × 2103 × 1585 pixels) that contains one large particle and 437,507 smaller particles. Smaller cubic image stacks of 1024, 512, 256, and 128 pixels wide used to test performance scaling behaviour are indicated on the parent volume as red squares.

The number of active CPU threads was set using the `-XX:ActiveProcessorCount=n` Java (OpenJDK 1.8.0_232) option (where n = 1, 2, 4, 8, 16, 32, 40, 20, 10, 5), to a maximum n of 40, which was the number of CPU threads present in the test system (Dell T7910, 282 GB DDR4 2400 MHz RAM in 16 DIMMs, dual Intel Xeon Silver 4114 CPUs at 2.20 GHz × 20 cores / 40 threads; Dell Hong Kong). For all tests 2-3 warm-up runs were performed to allow the just-in-time compiler to optimise code and the mean of 5 subsequent runs was recorded. Time t to complete particle labelling for each number of active CPU cores was plotted against image size in pixels p, power curves ($t \propto p^b$) fitted and the coefficient of determination (R^2) estimated (LibreOffice Calc v5.1.6.2). For comparison, times were recorded for the *s10up* image series with no hardware throttling using BoneJ's previous release (v6.1.1) and for the current code on a laptop (Latitude 7370, Dell UK).

Running code was sampled with Java VisualVM (Oracle; v. 1.8.0_221) to determine which methods were most expensive in terms of CPU time.

Each image from the *s10up* image series was opened in Avizo (v 2019.4, ThermoFisher), and a Connected Components analysis module attached to the opened data (image.am > Image Segmentation > Connected Components) with settings as close as possible to the new code's conditions (Gray image; Intensity: 20-255; Connectivity: Corner; Size: 1-0; Output: Label image; Output Type: Label Field (32 bit)). Avizo tests were performed on a Dell Precision T5820 tower with a single Intel Xeon W-2123 (4 cores, 8 threads) 3.6 GHz CPU, 64 GB 2666 MHz DDR4 RAM in 4 modules, and an 8 GB NVIDIA Quadro RTX4000 GPGPU, running Windows 10 (Microsoft).

Performance results

Particles are all correctly identified with no gaps between label numbers. The total number of particles in the test images agrees with the number expected, with previously validated versions of the software (Fig 3a), and with Avizo's Connected Components module. The *xz* spiral is labelled as a single particle, demonstrating correct label collision resolution among chunks. Scaling as a function of image size is approximately linear, i.e. O(n), with b = 0.918 – 1.068 and R^2 = 0.985 –

bioRxiv preprint doi: https://doi.org/10.1101/2020.02.28.969139; this version posted March 25, 2020. The copyright holder for this preprint (which was not certified by peer review) is the author/funder, who has granted bioRxiv a license to display the preprint in perpetuity. It is made available under aCC-BY 4.0 International license.

0.998 (Table 1; Fig. 3b). Scaling exponents < 1 indicate that larger images may be processed at a greater rate than smaller images.

active CPU threads	**scaling $t \propto p^b$**		**time to complete (s)**				
	b	***R²***	**2 MB**	**16 MB**	**128 MB**	**1 GB**	**6.5 GB**
1	1.068	0.996	0.133	0.996	8.198	69.38	865.7
2	1.040	0.998	0.086	0.535	4.406	50.40	358.0
4	1.013	0.994	0.068	0.341	2.554	29.36	226.2
5	0.987	0.992	0.068	0.303	2.149	23.88	181.3
8	0.957	0.988	0.067	0.286	1.560	19.60	142.7
10	0.964	0.988	0.057	0.232	1.432	14.56	134.6
16	0.941	0.988	0.059	0.217	1.377	13.57	111.4
20	0.946	0.991	0.058	0.238	1.519	14.18	116.3
32	0.918	0.985	0.067	0.208	1.342	13.84	97.5
40	0.947	0.993	0.046	0.249	1.247	14.58	95.1

Table 1. Scaling exponents (b), coefficients of determination (R^2) and completion times, calculated on the five *s10up* test images from 2×10^6 pixels (p) to 7×10^9 pixels, where time to complete $t = x + ap^b$. Scaling remains close to O(n) and in general improves as number of active threads increases. For all but the largest image, performance gains are marginal for more than 8-10 threads.

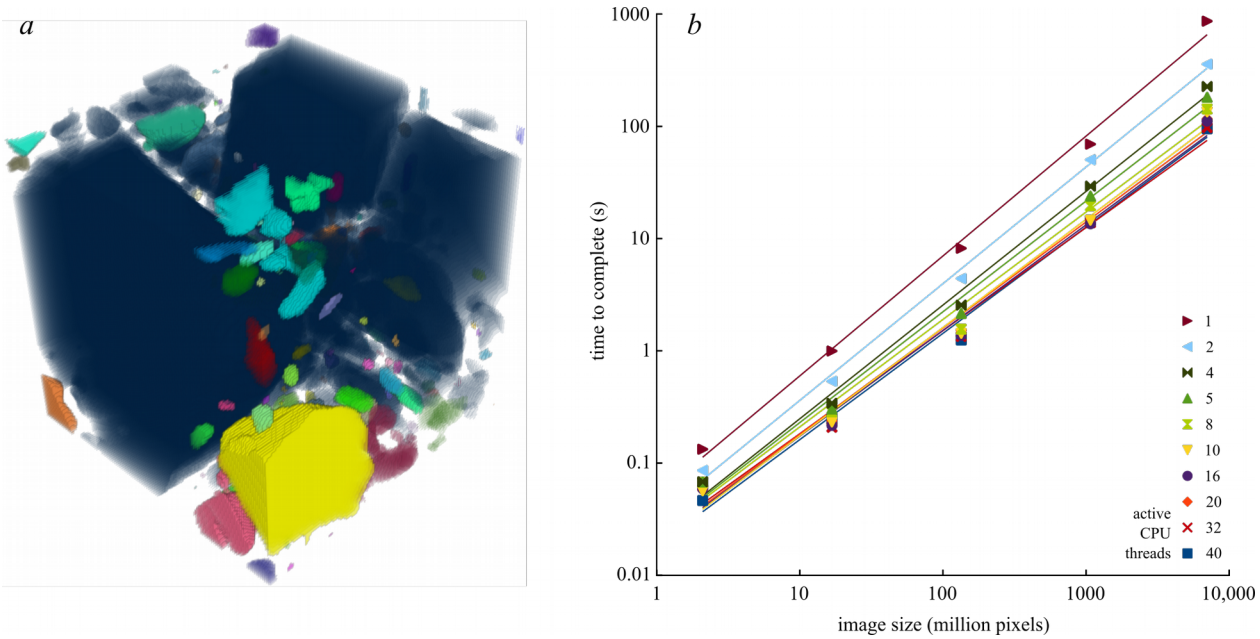

Figure 3: a) Volumetric rendering of the 2 MB *s10up* test image demonstrating correct labelling of regions, including those with complex connections that span multiple chunks. b) Performance scaling of two-pass multithreaded approach with bucket fountain collision resolution. Time to complete increases about linearly (O(n)) with increasing image size, and decreases with increasing number of active CPU threads. Note the slight decrease in gradient as number of CPU threads increases, indicating improving scaling to less than linear, but overlapping of regression lines for greater numbers of CPU threads cores indicating diminishing returns above 8-10 threads.

Processing speed in particles/s and pixels/s and overall finishing time saturates at around 8 - 16 CPUs on the test machine, depending on data size. The 128 MB test image was consistently fastest in pixels per second, perhaps because the image array size (512 × 512 pixels, 256kB slices) neatly matches the memory configuration leading to efficient data transfer.

bioRxiv preprint doi: https://doi.org/10.1101/2020.02.28.969139; this version posted March 25, 2020. The copyright holder for this preprint (which was not certified by peer review) is the author/funder, who has granted bioRxiv a license to display the preprint in perpetuity. It is made available under aCC-BY 4.0 International license.

Sampling indicated that `HashSet.add()` within `addNeighboursToMap()` is the biggest single user of CPU during first labelling pass (5-20%), while 'self time' within `firstIDAttribution()` also contributes a large fraction (80-95%).

The new implementation is 30 – 50× faster than the previous release (128 MB: 57 s; 1024 MB: 422 s; 6.5 GB: 2,891 s). On the laptop, completion times were tolerable (16 MB 0.534 s; 128 MB 4.2 s; 1024 GB: 37 s), but the 6.5 GB image caused an out of memory exception.

Discussion

This implementation of sequential region labelling achieves scaling at or below *O*(n). It may be relatively more efficient on larger images than on smaller images, perhaps through an accelerated rate of complexity reduction in larger more connected particles by *bucket fountain*, combined with Java's JIT compiler and adaptive optimisation increasing data throughput of larger arrays. The number of times data is retrieved from or written to RAM is minimised by accessing pixels non-recursively. Data reduction is achieved early by not storing redundant label collisions, and merging transitively connected labels efficiently with Java's `HashSet`. `HashSet.add()` is the most consuming of CPU wall-clock time, which may relate to instantiating and writing new `Integer` objects, or calculating their hashes. `HashSet` operations are minimised by the *bucket fountain*, which attempts to aggregate labels with the least handling of each `HashSet`'s contents by merging to the lowest bucket possible, with the side effect that some transitively linked labels are orphaned and must be recovered by a subsequent consistency check. An alternative, more careful implementation that joins all sub-regions in a single pass *snowballs* through consecutive buckets, merging each bucket's contents to the next lower (not the lowest) bucket referred to by its labels. The snowball approach makes completion times 20 – 100% longer than the bucket fountain in practice, presumably because each label is handled multiple times as the regions are aggregated as they pass through a larger number of buckets. Fast and sloppy with a small amount of recursive error correction noticeably outperforms slow and careful with no error correction in this case.

This multithreaded implementation of sequential region labelling displays memory-bound rather than CPU-bound behaviour and on the test system hits the so-called *memory wall* [22] at around 8-10 threads for smaller images of 1 GB and below. Performance would increase most readily as a function of increasing memory frequency and parallelism, which may require entirely new hardware architectures [23]. Future optimisations that reduce RAM access and improve utilisation of CPU cache, which is orders of magnitude faster than RAM, may ameliorate the current bottleneck.

Contemporary computers have benefited from algorithms implemented for General Purpose Graphical Processing Units (GPGPU) via NVIDIA's CUDA library or the OpenCL library. The main advantage of GPGPU processing is the large number of parallel data streams that can be processed and the high transfer rate within video RAM (VRAM; GDDR6 at c. 400 GB/s *vs* DDR4 RAM at c. 20 GB/s). It is therefore tempting to consider porting the current memory bandwidth-limited algorithm to exploit the GPGPU's parallel architecture. Unfortunately, at the time of writing OpenCL does not have a HashSet implementation, which is a core part of the label collision recording and resolution strategy. In addition, the time taken to read data from RAM into VRAM for GPGPU processing is unlikely to be substantially less than to read from RAM during CPU processing, however, this cost may be mitigated by the multiple pixel accesses during first pass labelling occurring on VRAM rather than RAM. Finally, available VRAM is typically much less than system RAM, with contemporary machines being able to hold up to 3 TB of RAM on a single motherboard (Dell 7920), but GPGPUs typically contain one or two orders of magnitude less VMRAM (NVIDIA QUADRO TX: 48 GB), severely constraining the maximum image size that could be handled by a GPGPU compared to CPU. Given the high performance of the CPU implementation, the cost:benefit of developing a GPU implementation requires careful consideration.

bioRxiv preprint doi: https://doi.org/10.1101/2020.02.28.969139; this version posted March 25, 2020. The copyright holder for this preprint (which was not certified by peer review) is the author/funder, who has granted bioRxiv a license to display the preprint in perpetuity. It is made available under aCC-BY 4.0 International license.

Java integers are 4-byte signed values. Using 0 as the background label and 1 as the minimum label gives a range of 2^{31} - 1 = 2,147,483,647 possible labels. It is possible to double the label range if Integer.MIN_VALUE (-2147483648) was used as the background value, and labels started from Integer.MIN_VALUE + 1, however in practice there are usually several orders of magnitude fewer particle labels required than pixels in the image: the 1GB test image contains over 1×10^9 pixels and fewer than 1×10^5 particles (about one particle per 10,000 pixels, which is one particle per cubic box of 21.5 pixels edge length). A practical consideration is that ImageJ displays integer arrays as RGB, which is unhelpful for later analysis: to avoid this the label image is converted to a 32-bit float, which is displayed as raw values with a colour LUT. Unfortunately, float loses integer precision for values higher than 2^{23}, which dramatically reduces the possible label range to a maximum of 8,388,608. Eight million labels is still sufficient for most images up to around $8\times10^6\times10^4$ or 8×10^{10}, about 80 GB. Should users have a need to process larger images containing more particles than these limits, the float precision restriction could be worked around.

Conclusion

This report describes an optimised implementation of sequential region labelling that fully exploits computational hardware resources and achieves linear (O(n)) or slightly better than linear scaling, providing connected components labelling of multi-GB images in a time scale of seconds to minutes instead of hours to days. It is provided as a working, easy to use package in BoneJ for ImageJ, as source code, and has an API for other developers to use.

Data availability

- BoneJ source code and changes: https://github.com/bonej-org/BoneJ2
- BoneJ release on Zenodo [24] doi:10.5281/zenodo.3726422
- Test images and performance testing results doi:10.6084/m9.figshare.11860542
- Test scripts doi:10.6084/m9.figshare.11860536

Funding

BoneJ2 infrastructure development was supported by a Wellcome Trust Biomedical Resource and Technology Development Grant (108442/Z/15/Z).

Competing interests

MD was a member of the Editorial Board of Royal Society Open Science at the time of submission and was not involved in the assessment of this submission.

Acknowledgements

Thank you to Robert Haase (MPI-CBG) for discussions and encouragement and to Alessandro Felder (UCL) and Richard Domander (RVC) for help with BoneJ2 engineering. I would be pleased to credit the (so far) anonymous originator of the *s10up* image that was used for testing this algorithm.

References

1. Burger W, Burge M. 2008 *Digital Image Processing: An Algorithmic Introduction Using Java*. 1st ed. New York: Springer.

2. Salehi A, Pircheraghi G, Foudazi R. 2019 Pore structure evolution during sintering of HDPE particles. *Polymer* **183**, 121865. (doi:10.1016/j.polymer.2019.121865)

bioRxiv preprint doi: https://doi.org/10.1101/2020.02.28.969139; this version posted March 25, 2020. The copyright holder for this preprint (which was not certified by peer review) is the author/funder, who has granted bioRxiv a license to display the preprint in perpetuity. It is made available under aCC-BY 4.0 International license.

3. Pires LF, Auler AC, Roque WL, Mooney SJ. 2020 X-ray microtomography analysis of soil pore structure dynamics under wetting and drying cycles. *Geoderma* **362**, 114103. (doi:10.1016/j.geoderma.2019.114103)

4. Krakowska P, Puskarczyk E, Jędrychowski M, Habrat M, Madejski P, Dohnalik M. 2018 Innovative characterization of tight sandstones from Paleozoic basins in Poland using X-ray computed tomography supported by nuclear magnetic resonance and mercury porosimetry. *J. Pet. Sci. Eng.* **166**, 389–405. (doi:10.1016/j.petrol.2018.03.052)

5. Li X, Akbarabadi M, Karpyn ZT, Piri M, Bazilevskaya E. 2015 Experimental investigation of carbon dioxide trapping due to capillary retention in saline aquifers. *Geofluids* **15**, 563–576. (doi:10.1111/gfl.12127)

6. Yio MHN, Wong HS, Buenfeld NR. 2019 3D pore structure and mass transport properties of blended cementitious materials. *Cem. Concr. Res.* **117**, 23–37. (doi:10.1016/j.cemconres.2018.12.007)

7. Guillermic R-M, Koksel F, Sun X, Hatcher DW, Nickerson MT, Belev GS, Webb MA, Page JH, Scanlon MG. 2018 Bubbles in noodle dough: Characterization by X-ray microtomography. *Food Res. Int.* **105**, 548–555. (doi:10.1016/j.foodres.2017.11.050)

8. Vennat E, Wang W, Genthial R, David B, Dursun E, Gourrier A. 2017 Mesoscale porosity at the dentin-enamel junction could affect the biomechanical properties of teeth. *Acta Biomater.* **51**, 418–432. (doi:10.1016/j.actbio.2017.01.052)

9. Wittig NK, Birkbak ME, Bach-Gansmo FL, Pacureanu A, Wendelboe MH, Brüel A, Thomsen JS, Birkedal H. 2019 No Signature of Osteocytic Osteolysis in Cortical Bone from Lactating NMRI Mice. *Calcif. Tissue Int.* **105**, 308–315. (doi:10.1007/s00223-019-00569-2)

10. Odgaard A, Gundersen HJG. 1993 Quantification of connectivity in cancellous bone, with special emphasis on 3-D reconstructions. *Bone* **14**, 173–182. (doi:10.1016/8756-3282(93)90245-6)

11. Han Y, Wagner RA. 1990 An efficient and fast parallel-connected component algorithm. *J. ACM* **37**, 626–642. (doi:10.1145/79147.214077)

12. Doube M, Kłosowski MM, Arganda-Carreras I, Cordelières F, Dougherty RP, Jackson J, Schmid B, Hutchinson JR, Shefelbine SJ. 2010 BoneJ: free and extensible bone image analysis in ImageJ. *Bone* **47**, 1076–1079. (doi:10.1016/j.bone.2010.08.023)

13. Cordelières FP, Jackson J. 2007 3D Object Counter. See https://imagej.nih.gov/ij/plugins/track/objects.html (accessed on 10 January 2020).

14. Bolte S, Cordelières FP. 2006 A guided tour into subcellular colocalization analysis in light microscopy. *J. Microsc.* **224**, 213–232. (doi:10.1111/j.1365-2818.2006.01706.x)

15. Schneider CA, Rasband WS, Eliceiri KW. 2012 NIH Image to ImageJ: 25 years of image analysis. *Nat. Methods* **9**, 671–675. (doi:10.1038/nmeth.2089)

16. Schindelin J *et al.* 2012 Fiji: an open-source platform for biological-image analysis. *Nat. Methods* **9**, 676–682. (doi:10.1038/nmeth.2019)

17. Torvalds L, Hamano J. 2016 *git*. See https://git-scm.com/.

bioRxiv preprint doi: https://doi.org/10.1101/2020.02.28.969139; this version posted March 25, 2020. The copyright holder for this preprint (which was not certified by peer review) is the author/funder, who has granted bioRxiv a license to display the preprint in perpetuity. It is made available under aCC-BY 4.0 International license.

18. Toriwaki J, Yonekura T. 2002 Euler number and connectivity indexes of a three dimensional digital picture. *Forma* **17**, 183–209.

19. Dougherty R, Kunzelmann K-H. 2007 Computing local thickness of 3D structures with ImageJ. *Microsc. Microanal.* **13**, 1678–1679. (doi:10.1017/S1431927607074430)

20. Arganda-Carreras I, Fernández-González R, Muñoz-Barrutia A, Ortiz-De-Solorzano C. 2010 3D reconstruction of histological sections: Application to mammary gland tissue. *Microsc. Res. Tech.* **73**, 1019–1029. (doi:10.1002/jemt.20829)

21. Schmid B, Schindelin J, Cardona A, Longair M, Heisenberg M. 2010 A high-level 3D visualization API for Java and ImageJ. *BMC Bioinformatics* **11**, 274. (doi:10.1186/1471-2105-11-274)

22. McKee SA, Wisniewski RW. 2011 Memory Wall. In *Encyclopedia of Parallel Computing* (ed D Padua), pp. 1110–1116. Boston, MA: Springer US. (doi:10.1007/978-0-387-09766-4_234)

23. Kingra SK, Parmar V, Chang C-C, Hudec B, Hou T-H, Suri M. 2020 SLIM: Simultaneous Logic-in-Memory Computing Exploiting Bilayer Analog OxRAM Devices. *Sci. Rep.* **10**, 1–14. (doi:10.1038/s41598-020-59121-0)

24. Richard Domander, Michael Doube, Curtis Rueden, Alessandro Felder, Mark Hiner, Jan Eglinger. 2020 *bonej-org/BoneJ2: styloid*. Zenodo. (doi:10.5281/zenodo.3726422)